GERMINAL CENTERS

Dynamic signaling by T follicular helper cells during germinal center B cell selection

Ziv Shulman,[1] Alexander D. Gitlin,[1] Jason S. Weinstein,[2] Begoña Lainez,[2]* Enric Esplugues,[3]* Richard A. Flavell,[3,4] Joseph E. Craft,[2,3] Michel C. Nussenzweig[1,4]†

T follicular helper (T_{FH}) cells select high-affinity, antibody-producing B cells for clonal expansion in germinal centers (GCs), but the nature of their interaction is not well defined. Using intravital imaging, we found that selection is mediated by large but transient contacts between T_{FH} and GC B cells presenting the highest levels of cognate peptide bound to major histocompatibility complex II. These interactions elicited transient and sustained increases in T_{FH} intracellular free calcium (Ca^{2+}) that were associated with T_{FH} cell coexpression of the cytokines interleukin-4 and -21. However, increased intracellular Ca^{2+} did not arrest T_{FH} cell migration. Instead, T_{FH} cells remained motile and continually scanned the surface of many GC B cells, forming short-lived contacts that induced selection through further repeated transient elevations in intracellular Ca^{2+}.

Germinal centers (GCs) are specialized microanatomical sites where B cells undergo clonal expansion, somatic hypermutation, and affinity maturation (*1*–*3*). Through iterative cycles of diversification and selection, the GC produces high-affinity memory B and plasma cells (*2*–*4*). Selection of high-affinity GC B cells requires their interaction with T follicular helper (T_{FH}) cells, which must discern among B cell clones according to their surface density of peptide–major histocompatibility complex II (pMHCII) (*5*). GC B cells are then programmed by T_{FH} cells to expand and hypermutate in direct proportion to the levels of cognate antigen presented (*6*). These events are controlled by T_{FH} cell–derived signals, including membrane-bound inducible costimulator (ICOS) and CD40L and the cytokines interleukin-4 (IL-4) and IL-21 (*7*, *8*), which are delivered in short-lived intercellular contacts (*9*).

To examine how the interactions between T_{FH} cells and GC B cells control selection, we imaged cells expressing genetically encoded fluorescent proteins in vivo by means of two-photon laser-scanning microscopy (TPLSM). Ovalbumin (OVA)–specific, T cell receptor (TCR) transgenic OT-II T cells expressing DsRed were adoptively transferred into congenic mice before priming with OVA in alum. After 2 to 3 weeks, a 95:5 mixture of nonfluorescent *Ly75*$^{-/-}$ and GFP^{+} *Ly75*$^{+/+}$ (*Ly75* encodes the cell-surface receptor DEC205) B cells, both specific for NP (4-hydroxy-3-nitrophenylacetyl; B1-8^{hi}) (*10*), was transferred before boosting with soluble OVA conjugated to NP (NP–OVA) (*11*, *12*). To induce selection, we increased the levels of pMHCII on the surface of GC B cells 7 to 8 days later through injection of DEC205 antibody fused to the cognate antigen OVA (αDEC-OVA) (Fig. 1A). This chimeric antibody targets DEC205, an endocytic receptor that carries associated proteins into MHCII-processing compartments of GC B cells (*5*). As a result, targeted GC B cells are initially retained in the GC light zone (LZ) and thereafter proliferate in the dark zone (DZ) (*5*, *6*). As a control, mice were injected with chimeric DEC205 antibody fused to an irrelevant antigen (*Plasmodium falciparum* circumsporozoite protein, αDEC-CS) (*5*). Popliteal lymph nodes were exposed after 4 to 10 hours, GCs were imaged by means of TPLSM (Fig. 1A), and the results were subjected to colocalization analysis (fig. S1).

Consistent with previous observations (*9*, *11*, *13*–*16*), GC lymphocytes were highly motile (T_{FH} cells, 9 μm/min and B cells, 6.6 μm/min) (Fig. 1, B and C, and movie S1). Under steady-state conditions, in which an unknown fraction of B cells are being positively selected, the majority of T-B contacts were short-lived (Fig. 1, B and D, and movie S1). Positive selection through αDEC-OVA injection was associated with a reduction in both GC B and T_{FH} cell velocities, along with an increase in the duration of the T-B contacts ($P < 0.0001$) (Fig. 1, B to D, and movies S2 and S3). In particular, the fraction of conjugates lasting 5 min or longer increased from 2.7 to 20.7% of the total interactions (Fig. 1D), and these occasionally moved at the B cell velocity (4.16 μm/min on average) (Fig. 1E). Although most of the conjugates moved short distances, and it was not possible to determine which one of the partners drags the other (movie S2), in those cases that could be interpreted the conjugates were led by the B cell and rarely, if at all, by the T cell (movie S3). Thus, even under conditions of enforced selection, most T-B interactions resembled those found under physiologic conditions in that they remained transient, with T cells forming and breaking contacts with multiple B cells (Fig. 1D and movie S3). Volume analysis of the T-B colocalized area revealed that the average contact size of the stable T-B conjugates (>5 min) was enlarged threefold during positive selection compared with control (Fig. 1F). As expected, polyclonal follicular B cells within the mantle zone did not slow down or form contacts with T_{FH} cells after αDEC-OVA injection (fig. S2 and movie S4). We conclude that positive selection through increased pMHCII on GC B cells is associated with longer but dynamic T-B contacts involving a larger surface area between the two interacting cells.

To examine whether positive selection interferes with the interactions between T_{FH} cells and GC B cells presenting low levels of pMHCII, we directly imaged selected and nonselected B cells within the same GC. GCs containing OT-II DsRed^{+} T cells and a mixture of B1-8^{hi} GFP^{+} *Ly75*$^{-/-}$, CFP^{+} *Ly75*$^{+/+}$, and nonfluorescent *Ly75*$^{-/-}$ B cells at a ~5:5:90 ratio were generated and imaged as in Fig. 1A. Positive selection of the B1-8^{hi} CFP^{+} *Ly75*$^{+/+}$ B cells was induced by injecting αDEC-OVA. When compared directly with *Ly75*$^{-/-}$ B cells presenting lower levels of pMHCII in the same GC, positively selected *Ly75*$^{+/+}$ B cells interacted for a longer time with T_{FH} cells ($P < 0.0001$) (Fig. 2, A and B, and movie S5) and formed a greater number of stable contacts (> 5 min) (Fig. 2C). However, selection of *Ly75*$^{+/+}$ GC B cells did not alter the behavior of nonselected *Ly75*$^{-/-}$ cells, which showed no significant change in contact duration or in the total number of interactions (> 0.5 min) with T_{FH} cells (Figs. 1D and 2, B and C, and movie S5). The majority of T_{FH} cells interacting with selected cells concurrently formed transient contacts with nonselected B cells (Fig. 2A and movie S5). We conclude that the increase in contact duration of T_{FH} cells with selected B cells does not substantially affect their interactions with nonselected B cells.

Our experiments indicate that increased contact size and duration correlates with the amount of pMHCII presented by GC B cells and their subsequent clonal expansion in the DZ (*6*), yet how these interactions affect T_{FH} T cell receptor (TCR) signaling is unknown. To examine the relationship between T-B contacts, TCR signaling, and B cell selection in the GC, we sought to measure intracellular Ca^{2+} levels in T_{FH} cells. Traditional Ca^{2+} dyes cannot be used for this purpose because T cells divide extensively and dilute such tracers before reaching the GC (*17*). To circumvent this issue, we used mice expressing a genetically encoded Ca^{2+} indicator (GCaMP3), which changes its fluorescence intensity according to intracellular Ca^{2+} levels (*18*, *19*). Lymphocytes from these mice showed an increase in intracellular fluorescence when stimulated with a Ca^{2+} ionophore or when stimulated through their antigen receptor (fig. S3 and movie S6).

Changes in Ca^{2+} fluorescence are best measured by comparison with a second dye that is insensitive to changes in intracellular Ca^{2+} levels.

[1]Laboratory of Molecular Immunology, The Rockefeller University, New York, NY 10065, USA. [2]Department of Internal Medicine (Rheumatology), School of Medicine, Yale University, New Haven, CT 06520, USA. [3]Department of Immunobiology, School of Medicine, Yale University New Haven, CT 06520, USA. [4]Howard Hughes Medical Institute (HHMI).
*Present address: Immunology Institute, Department of Medicine, Icahn School of Medicine at Mount Sinai, New York, NY 10029, USA.
†Corresponding author. E-mail: nussen@rockefeller.edu

Downloaded from www.sciencemag.org on November 1, 2015

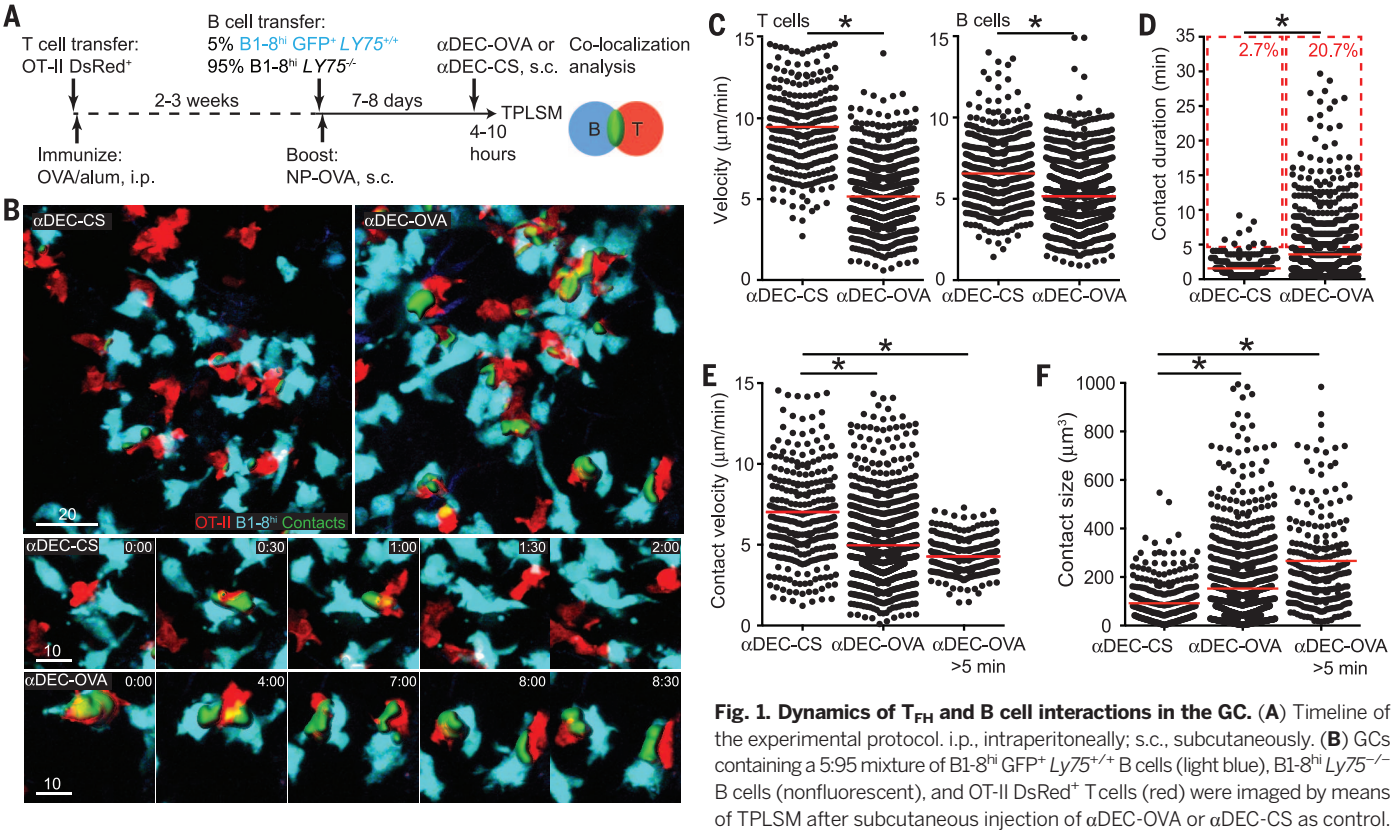

Fig. 1. Dynamics of T_{FH} and B cell interactions in the GC. (**A**) Timeline of the experimental protocol. i.p., intraperitoneally; s.c., subcutaneously. (**B**) GCs containing a 5:95 mixture of B1-8^{hi} GFP$^+$ *Ly75*$^{+/+}$ B cells (light blue), B1-8^{hi} *Ly75*$^{-/-}$ B cells (nonfluorescent), and OT-II DsRed$^+$ T cells (red) were imaged by means of TPLSM after subcutaneous injection of αDEC-OVA or αDEC-CS as control. T-B contacts (green) were detected by means of colocalization. Collapsed z-stacks of 40-μm depth (in 5-μm steps) are shown. (Bottom) T and B cell dynamics over time. Images correspond to movies S1 to S3. (**C**) Velocity analysis of OT-II T cells and B1-8^{hi} B cells in GCs. (**D**) T-B contact duration as measured by the lifetime of the T-B colocalized areas. Percentages indicate events lasting >5 min, marked by a dashed red box. (**E**) T-B conjugate velocity was measured as the velocity of the T-B colocalized area. (**F**) Contact size analysis as measured by T-B colocalized area. Each data point represents a single cell, and red lines represent mean values. Data in (C) to (F) were pooled from two to four mice imaged in two to four independent experiments. *$P < 0.0001$; two-tailed Student's *t* test.

Fig. 2. T_{FH} cell interactions with selected and non-selected GC B cells. (**A**) GCs containing a ~5:5:90 mixture of B1-8^{hi} CFP$^+$ *Ly75*$^{+/+}$ B cells (blue), B1-8^{hi} GFP$^+$ *Ly75*$^{-/-}$ (green), *Ly75*$^{-/-}$ nonfluorescent B cells, and OT-II DsRed$^+$ T cells (red) were imaged by means of TPLSM after subcutaneous injection of αDEC-OVA. Contacts between OT-II T cells and either B1-8^{hi} *Ly75*$^{+/+}$ or *Ly75*$^{-/-}$ B cells are shown in yellow and gray, respectively. 40-μm deep, collapsed z-stacks (5-μm steps) are shown. Arrowheads indicate B1-8^{hi} *Ly75*$^{+/+}$ and *Ly75*$^{-/-}$ GC B cells interacting simultaneously with one OT-II T cell. (**B**) Quantitation of contact duration between OT-II T cells and B1-8^{hi} *Ly75*$^{+/+}$ or *Ly75*$^{-/-}$ B cells. Each data point represents a single cell, and red lines represent mean values. Percentages indicate events >5 min, marked by a dashed red box. (**C**) The number of B cell contacts (>0.5 min, left; >5 min, right) with OT-II T cells was normalized to the number of B cells in each group. Exp., experiment. Data in (B) and (C) were pooled from four independent experiments. *$P < 0.0001$; two-tailed Student's *t* test.

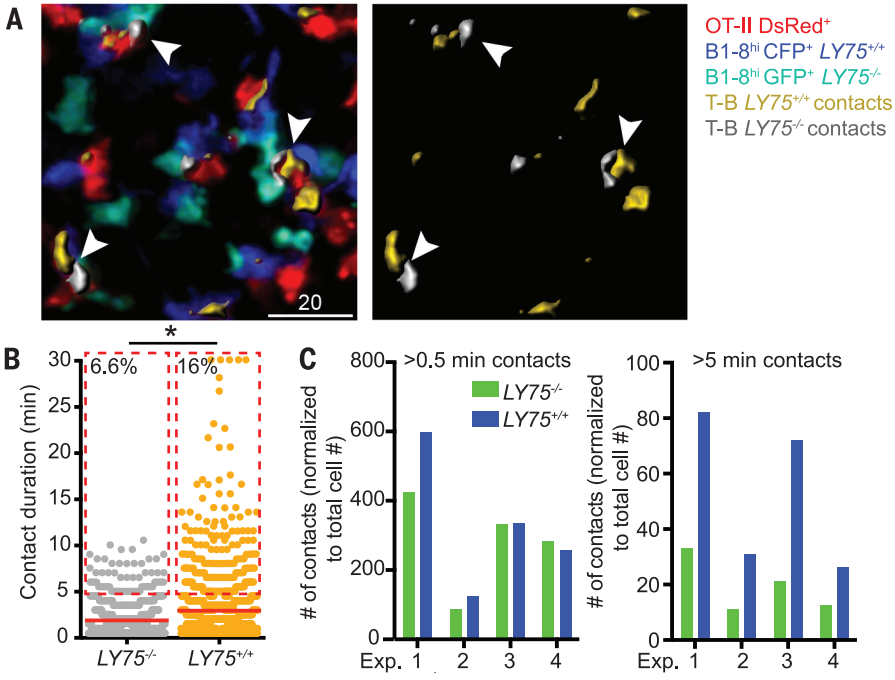

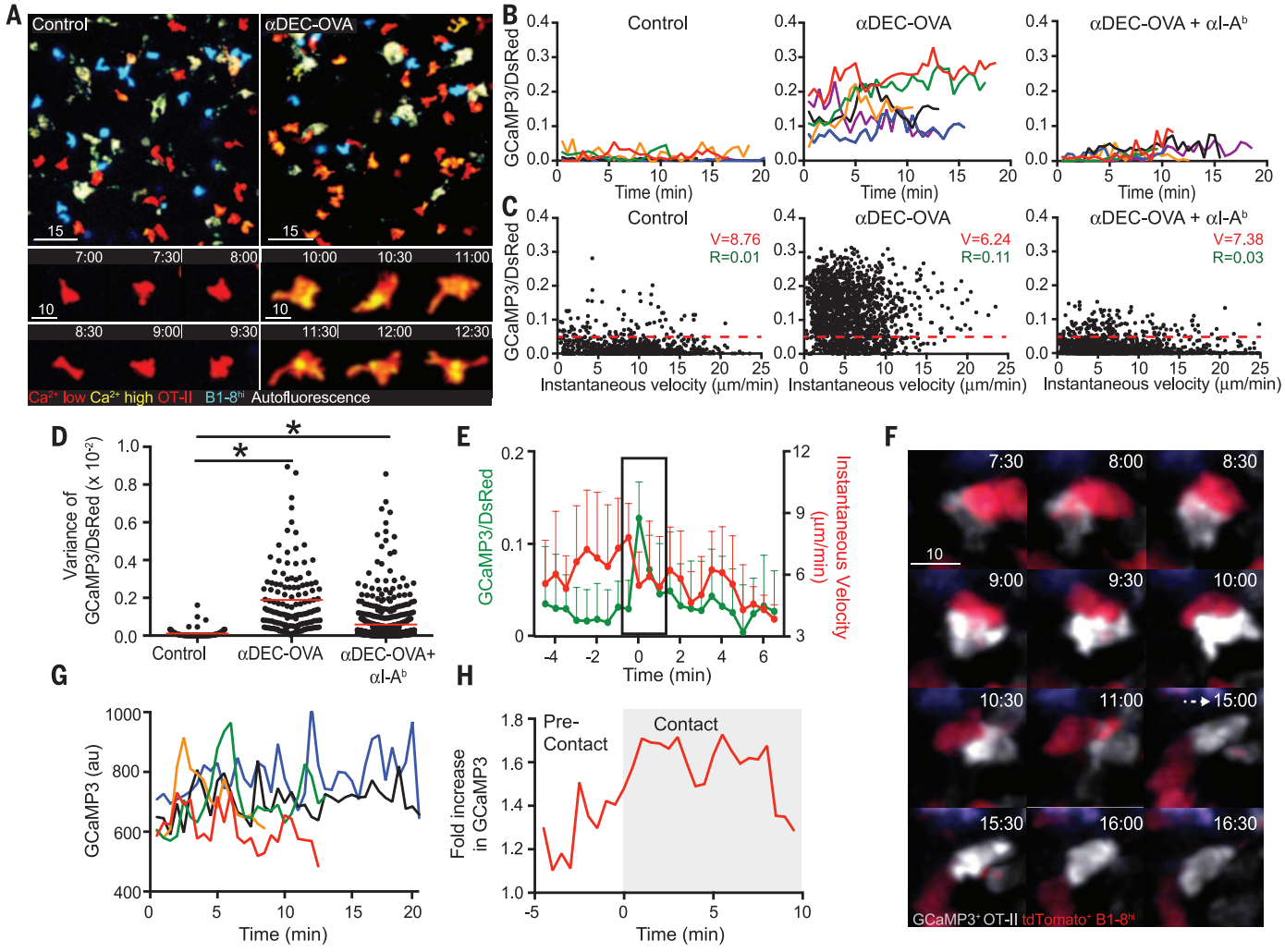

Fig. 3. T_{FH} cell Ca^{2+} signaling during B cell selection. (**A**) GCs containing a 5:95 mixture of B1-8^{hi} CFP^+ *Ly75*$^{+/+}$ B cells (light blue), B1-8^{hi} *Ly75*$^{-/-}$ B cells (nonfluorescent), and OT-II $DsRed^+$ $GCaMP3^+$ T cells (red, Ca^{2+} low; yellow, Ca^{2+} high) were imaged by TPLSM in untreated mice or after subcutaneous injection of αDEC-OVA. (Bottom) Dynamic changes in GCaMP3 fluorescence in individual OT-II T cells over time. (**B**) Traces show changes in the GCaMP3/DsRed ratios over time for six single T cells in each condition. αI-A^b was injected intravenously after αDEC-OVA injection. (**C**) Scatter plots depict the GCaMP3/DsRed ratio versus instantaneous velocity as measured at successive 30-s intervals. Each dot represents a single cell at a single time point. Average velocity (*V*) and GCaMP3/DsRed ratios (*R*) of two to three experiments are indicated in red and green, respectively. (**D**) GCaMP3/DsRed ratio fluctuations in single cells (expressed as variance) under control and αDEC-OVA conditions. (**E**) GCaMP3/DsRed spikes of nine cells were synchronized. Traces of average GCaMP3/DsRed ratios and corresponding instantaneous velocities are shown. The synchronized spikes fall in the black rectangle. Error bars indicate SEM. (**F**) OT-II $GCaMP3^+$ T cells and B1-8^{hi} $tdTomato^+$ *Ly75*$^{+/+}$ B cells were imaged in GCs over time as in (A). Images correspond to movie S11. (**G**) Traces show GCaMP3 mean fluorescence intensities for five OT-II T cells in contact with B1-8^{hi} $tdTomato^+$ *Ly75*$^{+/+}$ GC B cells. (**H**) Initiation of contacts were synchronized in 4 OT-II $GCaMP3^+$ T cells, and the corresponding average of GCaMP3 fluorescence intensity was traced before and during the contact (au, arbitrary units). Data are representative of two or three mice imaged in two or three independent experiments. *$P < 0.0001$; two-tailed Student's *t* test.

We therefore induced and imaged GCs, as described in Fig. 1A, using OT-II $GCaMP3^+$ $DsRed^+$ T cells and measured the ratio of GCaMP3:DsRed fluorescence intensity (fig. S4). To determine whether T_{FH} cell Ca^{2+} content is associated with changes in cellular dynamics, velocities at successive time points were measured (instantaneous velocity) and correlated with intracellular Ca^{2+} content (*17*). Under steady-state conditions, spikes in Ca^{2+} content in GC T_{FH} cells were rare (Fig. 3, A to C; fig. S5A; and movie S7). In contrast, αDEC-OVA injection increased the proportion of GC T_{FH} cells with GCaMP3:DsRed ratios above 0.05 from 9 to 68% (Fig. 3, A to C, and movie S7) and the average ratio by 8.3-fold (fig. S5A). Single T_{FH} cells that were actively engaged in B cell selection showed sustained increases in intracellular Ca^{2+} over time, which did not drop to control levels during the observation period (Fig. 3B). In addition, single T_{FH} cells also displayed frequent Ca^{2+} spike transients (Fig. 3, B and D). Both sustained and transient increases in T_{FH} intracellular Ca^{2+} levels were a result of TCR:pMHCII interactions (Fig. 3, B to D, and fig. S5A). We conclude that selection is associated with TCR:pMHCII–dependent increases in T_{FH} cell Ca^{2+} content that were both transient and long-term.

Increases in intracellular Ca^{2+} content in naïve T cells result in motility arrest and enhanced effector functions (*17*, *20*, *21*). By correlating intracellular Ca^{2+} content and instantaneous velocity in unperturbed GCs, we found that T_{FH} cells moved at an average speed of 8.76 μm/min regardless of their Ca^{2+} content (Fig. 3C and fig. S5B). Consistently, in αDEC-OVA–targeted GCs the velocity of T_{FH} cells with high- and low-Ca^{2+} content was decreased to an average of 6.24 μm/min, and few, if any, of the actively engaged T_{FH} cells stopped moving or lost their morphological polarity while signaling (Fig. 3C, fig. S5B, and movies S7 to S9). However, there was no

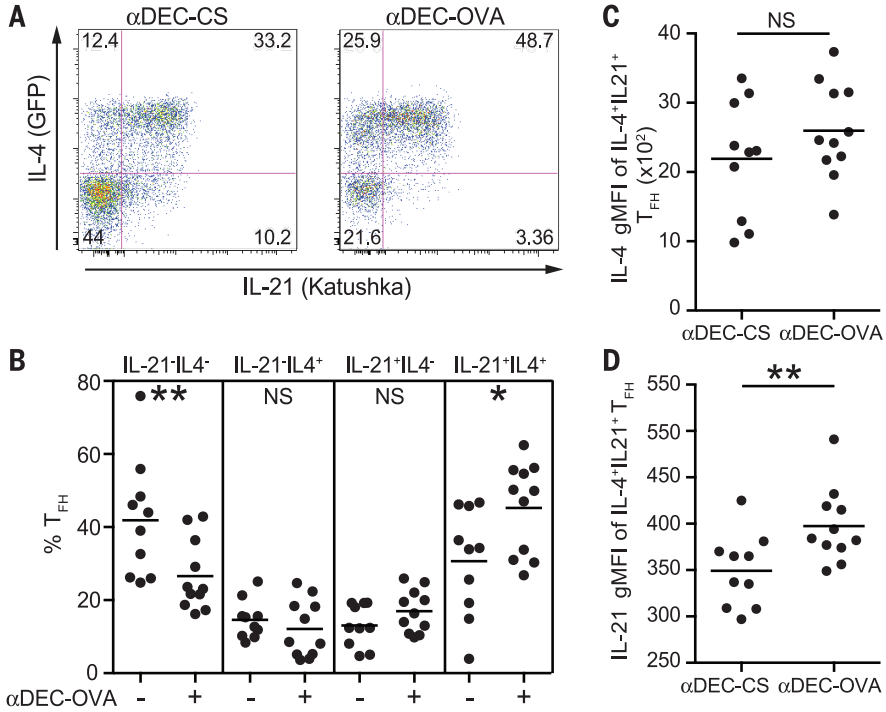

Fig. 4. Multifunctional T_{FH} cells during B cell selection. (**A** and **B**) $CD4^+$ T cells derived from OVA-immunized *Il4-IRES-GFP* and *Il21-IRES-Katushka* double knock-in mice and a 5:95 ratio of B1-8^{hi} *Ly75*$^{+/+}$ and *Ly75*$^{-/-}$ B cells were transferred into TCRβ-deficient mice, before boosting with NP-OVA. After 7 days, mice were injected with αDEC-CS or αDEC-OVA, and lymph nodes were analyzed 9 hours later. The proportions of cytokine-expressing cells among T_{FH} ($CD8^-$, $B220^-$, $CD4^+$, $CD44^+$, $CD62L^-$, $CXCR5^{high}$, and $PD\text{-}1^{high}$) subsets are indicated. (**C** and **D**) gMFI of IL-4 (C) or IL-21 (D) reporter expression. Each data point represents a single mouse, and lines represent mean values. Pooled data from three experiments each with three or four mice per condition. *P = 0.025; **P = 0.014; ***P = 0.02; two-tailed Student's t test. NS, not significant.

clear correlation between the level of Ca^{2+} increase and cell motility because both T_{FH} cells with high- and low-Ca^{2+} content had the same average velocity (Fig. 3C, fig. S5B, and movie S7). Nevertheless, by synchronizing transient small Ca^{2+} peaks of several T_{FH} cells, we found that these were precisely associated with a reduction in instantaneous velocity of ~2.5 μm/min (Fig. 3E, fig. S6, and movie S10).

Given these broad changes in Ca^{2+} content and the regulated T-B interactions, we sought to examine T_{FH} intracellular Ca^{2+} levels during the formation of T-B contacts. To this end, we imaged selection in GCs containing a 95:5 mixture of B1-8^{hi} nonfluorescent *Ly75*$^{-/-}$ B cells, tdTomato$^+$ *Ly75*$^{+/+}$ B cells, and OT-II GCaMP3$^+$ T cells. Injection of αDEC-OVA induced the formation of T cell contacts with *Ly75*$^{+/+}$ B cells that were associated with transient spikes in T_{FH} intracellular Ca^{2+} content (Fig. 3, F and G, and movies S11 and S12). To determine whether these Ca^{2+} transients take place preferentially during T-B conjugate formation, we synchronized clearly isolated contact events and measured the average GCaMP3 fluorescence intensity in T_{FH} cells before and during these interactions. Although the intracellular Ca^{2+} levels in T_{FH} cells were high in αDEC-OVA–targeted GCs (Fig. 3B), an additional small increase at the onset of contact with selected B cells was detected (Fig. 3H and movie S10).

Changes in intracellular Ca^{2+} concentration control T cell effector functions, including the expression of IL-4 and IL-21 (*20*, *22*), both of which are required for effective B cell immune responses (*23*). T effector cells can express either or both of these cytokines, and this multifunctionality is associated with enhanced immunity and vaccine responses (*24*–*28*). To determine whether the long-term increase in T_{FH} intracellular Ca^{2+} levels alters the quality of GC T_{FH} cells, we examined T cells derived from IL4/IL21 double reporter mice expressing *Il4-IRES-GFP* (*29*) and *Il21-IRES-Katushka* (fig. S7). Polyclonal OVA-primed $CD4^+$ T cells isolated from these mice were adoptively transferred into TCRβ-deficient mice along with B1-8^{hi} *Ly75*$^{+/+}$ and *Ly75*$^{-/-}$ B cells at a 5:95 ratio. Recipients were boosted with NP-OVA and injected 7 days later with either αDEC-CS or αDEC-OVA so as to induce selection. T_{FH} cells were examined for cytokine expression 9 hours later by means of flow cytometry. αDEC-OVA injection resulted in a significant decrease in IL-4^-IL-21^- T_{FH} cells and a concomitant increase in IL-4^+IL-21^+ multifunctional T_{FH} cells in the absence of cell division or a significant change in the number of single-cytokine-producing cells (Fig. 4, A and B, and fig. S8). Moreover, there was also a small but significant increase in the amount of IL-21, but not IL-4, produced by the double-positive cells, as measured by an increase in the mean fluorescence intensity of the reporters (Fig. 4, C and D). Thus, increased T_{FH} Ca^{2+} signaling during B cell selection is associated with a rapid change in the quality of the GC T_{FH} response, with increased development of multifunctional T_{FH} cells producing Ca^{2+}–dependent cytokines.

Our results demonstrate that T_{FH} cells respond to pMHCII on GC B cells during selection differently than the prolonged interactions of T cells with dendritic cells (DCs) in the T zone or with B cells at the T-B border (*30*–*36*). The transient interactional dynamics of T_{FH} cells in GCs allow them to continuously seek and find B cells presenting high levels of pMHCII and provide them with preferential help while permitting competitive opportunities for other GC B cells. This mode of B cell scanning allows T_{FH} cells to interact with many cells presenting a range of pMHCII levels, rather than forming a prolonged contact with a single high-affinity B cell.

Our experiments show that the increased size and duration of contacts between GC T_{FH} and selected B cells prolongs Ca^{2+} signaling and modifies the quality of the GC T_{FH} response. These events induce coexpression of the Ca^{2+}-dependent cytokines IL-4 and IL-21, which endow T_{FH} cells with effector capabilities that facilitate high-affinity B cell selection.

REFERENCES AND NOTES

1. C. Berek, A. Berger, M. Apel, *Cell* **67**, 1121–1129 (1991).
2. C. D. Allen, T. Okada, J. G. Cyster, *Immunity* **27**, 190–202 (2007).
3. G. D. Victora, M. C. Nussenzweig, *Annu. Rev. Immunol.* **30**, 429–457 (2012).
4. M. Oprea, A. S. Perelson, *J. Immunol.* **158**, 5155–5162 (1997).
5. G. D. Victora *et al.*, *Cell* **143**, 592–605 (2010).
6. A. D. Gitlin, Z. Shulman, M. C. Nussenzweig, *Nature* **509**, 637–640 (2014).
7. S. Crotty, *Annu. Rev. Immunol.* **29**, 621–663 (2011).
8. C. G. Vinuesa, J. G. Cyster, *Immunity* **35**, 671–680 (2011).
9. C. D. Allen, T. Okada, H. L. Tang, J. G. Cyster, *Science* **315**, 528–531 (2007).
10. T. A. Shih, M. Roederer, M. C. Nussenzweig, *Nat. Immunol.* **3**, 399–406 (2002).
11. T. A. Schwickert *et al.*, *Nature* **446**, 83–87 (2007).
12. Materials and methods are available as supplementary materials on *Science* Online.
13. A. E. Hauser *et al.*, *Immunity* **26**, 655–667 (2007).
14. M. Kitano *et al.*, *Immunity* **34**, 961–972 (2011).
15. S. M. Kerfoot *et al.*, *Immunity* **34**, 947–960 (2011).
16. Z. Shulman *et al.*, *Science* **341**, 673–677 (2013).
17. S. H. Wei *et al.*, *J. Immunol.* **179**, 1586–1594 (2007).
18. J. Nakai, M. Ohkura, K. Imoto, *Nat. Biotechnol.* **19**, 137–141 (2001).
19. H. A. Zariwala *et al.*, *J. Neurosci.* **32**, 3131–3141 (2012).

20. S. Agarwal, O. Avni, A. Rao, *Immunity* **12**, 643–652 (2000).
21. P. A. Negulescu, T. B. Krasieva, A. Khan, H. H. Kerschbaum, M. D. Cahalan, *Immunity* **4**, 421–430 (1996).
22. H. P. Kim, L. L. Korn, A. M. Gamero, W. J. Leonard, *J. Biol. Chem.* **280**, 25291–25297 (2005).
23. K. Ozaki *et al.*, *Science* **298**, 1630–1634 (2002).
24. M. R. Betts *et al.*, *Blood* **107**, 4781–4789 (2006).
25. E. W. Newell, N. Sigal, S. C. Bendall, G. P. Nolan, M. M. Davis, *Immunity* **36**, 142–152 (2012).
26. P. A. Darrah *et al.*, *Nat. Med.* **13**, 843–850 (2007).
27. M. A. Kroenke *et al.*, *J. Immunol.* **188**, 3734–3744 (2012).
28. K. Lüthje *et al.*, *Nat. Immunol.* **13**, 491–498 (2012).
29. M. Mohrs, K. Shinkai, K. Mohrs, R. M. Locksley, *Immunity* **15**, 303–311 (2001).
30. T. R. Mempel, S. E. Henrickson, U. H. Von Andrian, *Nature* **427**, 154–159 (2004).
31. G. Shakhar *et al.*, *Nat. Immunol.* **6**, 707–714 (2005).
32. M. J. Miller, S. H. Wei, I. Parker, M. D. Cahalan, *Science* **296**, 1869–1873 (2002).
33. D. Skokos *et al.*, *Nat. Immunol.* **8**, 835–844 (2007).
34. T. Okada *et al.*, *PLOS Biol.* **3**, e150 (2005).
35. H. Qi, J. L. Cannons, F. Klauschen, P. L. Schwartzberg, R. N. Germain, *Nature* **455**, 764–769 (2008).
36. T. A. Schwickert *et al.*, *J. Exp. Med.* **208**, 1243–1252 (2011).

ACKNOWLEDGMENTS

We thank G. Victora for helpful discussions and suggestions, D. Bosque and T. Eisenreich for help with mouse colony management, A. Abadir for protein production, and K. Yao for technical help. The data reported in this manuscript are tabulated in the main paper and in the supplementary materials. Z.S. is a Human Frontiers of Science Program fellow (reference LT000340/2011-L). A.D.G. is supported by NIH Medical Scientist Training Program grant T32GM07739 to the Weill Cornell/Rockefeller/Sloan-Kettering Tri-Institutional MD-PhD Program. Support for the Rockefeller University multiphoton microscope was granted by the Empire State Stem Cell Fund through New York State Department of Health contract C023046. This work was supported by NIH grants AI037526-19, AI072529-06, and AI100663-02 to M.C.N. and NIH grants AR40072-24 and AR053495-08 (the content is solely the responsibility of the authors and does not necessarily represent the official views of the NIH) and the Alliance for Lupus Research to J.E.C. M.C.N. and R.A.F. are HHMI investigators.

SUPPLEMENTARY MATERIALS

www.sciencemag.org/content/345/6200/1058/suppl/DC1
Materials and Methods
Figs. S1 to S8
References
Movies S1 to S12

24 June 2014; accepted 31 July 2014
10.1126/science.1257861

CELL MIGRATION IN 3D

Generation of compartmentalized pressure by a nuclear piston governs cell motility in a 3D matrix

Ryan J. Petrie,[1]* Hyun Koo,[1,2,3] Kenneth M. Yamada[1]*

Cells use actomyosin contractility to move through three-dimensional (3D) extracellular matrices. Contractility affects the type of protrusions cells use to migrate in 3D, but the mechanisms are unclear. In this work, we found that contractility generated high-pressure lobopodial protrusions in human cells migrating in a 3D matrix. In these cells, the nucleus physically divided the cytoplasm into forward and rear compartments. Actomyosin contractility with the nucleoskeleton-intermediate filament linker protein nesprin-3 pulled the nucleus forward and pressurized the front of the cell. Reducing expression of nesprin-3 decreased and equalized the intracellular pressure. Thus, the nucleus can act as a piston that physically compartmentalizes the cytoplasm and increases the hydrostatic pressure between the nucleus and the leading edge of the cell to drive lamellipodia-independent 3D cell migration.

Cells moving across a flat two-dimensional (2D) surface or inside nonlinearly elastic 3D collagen use polarized signaling to direct the formation of a dendritic actin network and extend flat, lamellipodial protrusions (*1*, *2*). When primary human fibroblasts move within a cross-linked, linearly elastic 3D structure such as dermal or cell-derived matrix, they can switch to a lamellipodia-independent migration mechanism characterized by nonpolarized signaling and blunt, cylindrical protrusions termed "lobopodia" (*1*). Actomyosin contractility via the RhoA–ROCK–myosin II signaling axis is required for cells to form and maintain lobopodia in response to the degree of matrix cross-linking. However, the mechanism by which increased contractility generates lobopodia is unclear.

Lobopodial cells can also be distinguished by rapid membrane blebbing along their sides, oriented perpendicular to the leading edge. Membrane blebs can be generated by elevated intracellular hydrostatic pressure, local weakening of the attachment of the plasma membrane to the underlying cortex, or both (*3*–*5*). We hypothesized that this lateral blebbing could result from elevated intracellular pressure during lobopodial motility. This increased pressure might result from the RhoA, ROCK, and myosin II activities required for the lamellipodia-independent migration of fibroblasts through a physiological linearly elastic 3D matrix (*1*).

We tested the hypothesis by directly determining intracellular pressures in primary human fibroblasts migrating on 2D surfaces compared with a 3D extracellular matrix (ECM). We used a microelectrode coupled to a servo-null micropressure system to penetrate the plasma membrane immediately in front of the nucleus (relative to the leading edge) and to measure the intracellular hydrostatic pressure exerted by the cytoplasm directly (P_{ic}) (Fig. 1) (see supplementary materials and methods). Direct comparisons of pressure in cells migrating on top of a cell-derived matrix (CDM) and embedded within a 3D collagen matrix revealed low hydrostatic pressures in both 2D and 3D lamellipodial cells [~300 and 700 Pa on the linearly elastic 2D surface of the CDM and within nonlinearly elastic 3D collagen, respectively; see (*1*) for characterization of matrix elastic behavior]. In contrast, intracellular pressure was substantially elevated (~2200 Pa) in lobopodial cells migrating inside the 3D CDM. Switching these lobopodial cells to lamellipodial cells by inhibiting RhoA, ROCK, or myosin II (*1*) reduced hydrostatic pressure (to ~400 Pa) in each case. This inhibition distinguished lobopodia from the contractility-independent water permeation mechanism used by certain cancer cells

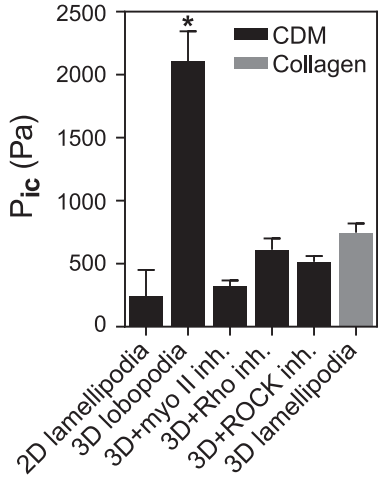

Fig. 1. Actomyosin contractility governs intracellular pressure in a 3D ECM. Comparison of the intracellular pressures ($n \geq 20$ replicates each) of lamellipodial cells on 2D CDM and in 3D collagen, untreated lobopodial cells in 3D CDM, or cells in CDM treated overnight with inhibitors of myosin II (25 μM blebbistatin), ROCK (10 μM Y-27632), or RhoA (10 μg/ml C3 transferase). $N = 3$ independent experiments, $^*P < 0.001$. Error bars indicate SEM.

[1]Laboratory of Cell and Developmental Biology, National Institute of Dental and Craniofacial Research, National Institutes of Health, Bethesda, MD 20892–4370, USA. [2]Center for Oral Biology, Department of Microbiology and Immunology, University of Rochester Medical Center, Rochester, NY 14642, USA. [3]Biofilm Research Labs, Levy Center for Oral Health, Department of Orthodontics, University of Pennsylvania School of Dental Medicine, Philadelphia, PA 19104–6030, USA.
***Corresponding author. E-mail: petrier@mail.nih.gov (R.J.P.); kyamada@mail.nih.gov (K.M.Y.)**

Science
AAAS

Dynamic signaling by T follicular helper cells during germinal center B cell selection

Ziv Shulman *et al.*

Science **345**, 1058 (2014);
DOI: 10.1126/science.1257861

This copy is for your personal, non-commercial use only.

If you wish to distribute this article to others, you can order high-quality copies for your colleagues, clients, or customers by clicking here.

Permission to republish or repurpose articles or portions of articles can be obtained by following the guidelines here.

The following resources related to this article are available online at www.sciencemag.org (this information is current as of November 1, 2015):

Updated information and services, including high-resolution figures, can be found in the online version of this article at:
http://www.sciencemag.org/content/345/6200/1058.full.html

Supporting Online Material can be found at:
http://www.sciencemag.org/content/suppl/2014/08/27/345.6200.1058.DC1.html

This article **cites 35 articles**, 11 of which can be accessed free:
http://www.sciencemag.org/content/345/6200/1058.full.html#ref-list-1

This article has been **cited by** 9 articles hosted by HighWire Press; see:
http://www.sciencemag.org/content/345/6200/1058.full.html#related-urls

This article appears in the following **subject collections:**
Immunology
http://www.sciencemag.org/cgi/collection/immunology

Downloaded from www.sciencemag.org on November 1, 2015

Science (print ISSN 0036-8075; online ISSN 1095-9203) is published weekly, except the last week in December, by the American Association for the Advancement of Science, 1200 New York Avenue NW, Washington, DC 20005. Copyright 2014 by the American Association for the Advancement of Science; all rights reserved. The title *Science* is a registered trademark of AAAS.